



## ISTITUTO NAZIONALE DI RICERCA METROLOGICA Repository Istituzionale

Effective versus standard Epstein loss figure in Fe-Si sheets.

This is the author's accepted version of the contribution published as:

*Original*

Effective versus standard Epstein loss figure in Fe-Si sheets / Ferrara, Enzo; Appino, Carlo; Rocchino, Luciano; Ragusa, Carlo; de la Barrière, Olivier; Fiorillo, Fausto. - In: INTERNATIONAL JOURNAL OF APPLIED ELECTROMAGNETICS AND MECHANICS. - ISSN 1383-5416. - 55:(2017). [10.3233/JAE-172263]

*Availability:*

This version is available at: 11696/57002 since: 2021-02-07T06:36:20Z

*Publisher:*

IOS Press:Nieuwe Hemweg

*Published*

DOI:10.3233/JAE-172263

*Terms of use:*

Visibile a tutti

This article is made available under terms and conditions as specified in the corresponding bibliographic description in the repository

*Publisher copyright*

(Article begins on next page)

## **Effective versus standard Epstein loss figure in Fe-Si sheets.**

Enzo Ferrara<sup>1</sup>, Carlo Appino<sup>1</sup>, Luciano Rocchino<sup>1</sup>, Carlo Ragusa<sup>2</sup>,  
Olivier de la Barrière<sup>3</sup>, and Fausto Fiorillo<sup>1</sup>

<sup>1</sup> *Istituto Nazionale di Ricerca Metrologica, Nanoscience and Materials Division, Torino, Italy*

<sup>2</sup> *Politecnico di Torino, Energy Department, Torino, Italy*

<sup>3</sup> *SATIE-ENS, UniverSud, Cachan, France*

## Abstract

The magnetic power losses have been measured at 50 Hz and different peak polarization values on different types of non-oriented and grain-oriented Fe-Si sheets using the Epstein frame, according to the current standards. The very same measurements have then been repeated by measuring polarization and tangential magnetic field by means of localized windings, centrally placed on the strips inside the Epstein frame windings, thereby retrieving the effective field and the true power loss figure. It is obtained that the ratio of the standard  $P_{\text{epst}}$  to the effective  $P_{\text{eff}}$  loss figure, which can be interpreted in terms of ratio of effective  $l_{\text{eff}}$  to conventional ( $l_m = 0.94$  m) magnetic path length, evolves with the peak polarization  $J_p$ , showing, in general, a monotonic increase with increasing  $J_p$ . The deviation of  $P_{\text{epst}}$  from  $P_{\text{eff}}$  is observed to range from about -3 % in the non-oriented alloys at low inductions to about +5 % in the grain-oriented alloys at  $J_p = 1.8$  T. This behavior finds a rationale in the existence of a polarization profile  $J_p(x)$  measured along the strip length and in the dependence of  $P_{\text{eff}}$  on  $J_p$ , showing a power law  $P_{\text{eff}}(J_p) \propto J_p^n$ , with  $n > 1$  and increasing with  $J_p$ . The so calculated effective path length  $l_{\text{eff}} = l_m \cdot P_{\text{epst}} / P_{\text{eff}}$  consistently show a monotonic increase with  $J_p$ , which is more relevant in the GO alloys.

Keywords: Magnetic power losses, Epstein frame, Magnetic steels.

## 32 1. Introduction

33 The 25 cm Epstein test-frame with a defined magnetic path length  $l_m = 0.94$  m is a solidly assessed method for  
34 the characterization of the magnetic steel sheets. It ensures good measurement reproducibility and is widely  
35 adopted as an industry standard [1][2][3][4]. It is also well established that the specific features of the employed  
36 magnetic circuit, with the double overlapping corners and the ensuing inhomogeneous flux distribution, make the  
37 value of the measured quantities, namely the magnetic losses, different from the value of the true quantities [5][6].  
38 True values could, however, be possibly accounted for by incorporating the complex response of the magnetic  
39 circuit into an effective magnetic path length  $l_{\text{eff}}$ , depending on the type of sheet, peak induction value, frequency,  
40 and type of excitation [7]. Should the effective (true) power loss figure  $P_{\text{eff}}$  be measured, one could express it in  
41 terms of standard power loss value  $P_{\text{epst}}$  according to

$$42 \quad P_{\text{eff}} = P_{\text{epst}} \cdot l_m / l_{\text{eff}}. \quad (1)$$

43 Measurements of  $P_{\text{eff}}$  using a single strip tester and an  $H$ -coil were reported for non-oriented (NO) and  
44 grain-oriented (GO) sheets by Ahlers, et al. [8]. They found at 50 Hz  $P_{\text{epst}} < P_{\text{eff}}$ , that is  $l_{\text{eff}} > l_m$  in all materials,  
45 with maximum difference of the order of 8% in GO sheets at  $J_p = 1.7$  T. These authors justified their results in  
46 terms of effective length, expressed as  $l_{\text{eff}} = l_0 + (\mu_l/2\mu_c) \cdot l_c$ , the sum of the legs length  $l_0$  and part of the corners  
47 length  $l_c$ , depending on the ratio of the leg to corner permeabilities  $\mu_l$  and  $\mu_c$ . A number of literature experiments  
48 [5] actually show scattered outcomes, both in NO and GO materials, with  $P_{\text{epst}}$  either higher or lower than  $P_{\text{eff}}$  and  
49  $P_{\text{epst}} / P_{\text{eff}}$  generally decreasing with the peak polarization  $J_p$ . Marketos, et al. [7][9] have determined  $l_{\text{eff}}$  by  
50 measuring GO and NO sheets with conventional 25 cm and reduced 17.5 cm Epstein frames. They find, assuming  
51 identical flux distribution in the corners of the two frames, that  $l_{\text{eff}}$  is always higher than  $l_m$  (that is,  $P_{\text{epst}} / P_{\text{eff}} > 1$ )  
52 in GO high-permeability sheets and, in contrast with the results reported in [5], increasing with  $J_p$ .

53 In this paper we discuss measurements of power losses performed at 50 Hz on different types of NO and GO  
54 steel sheets, both according to the measuring standard (25 cm Epstein frame with  $l_m = 0.94$  m) and by detecting  
55 the tangential field and the induction derivative by collinear narrow  $H$ - and  $B$ -coils windings, placed directly upon  
56 the steel strips at the centre of the Epstein legs. In this way, the true power loss  $P_{\text{eff}}(J_p)$  is obtained in comparison  
57 with the standard loss figure  $P_{\text{epst}}(J_p)$ . A ratio  $P_{\text{epst}} / P_{\text{eff}}$  monotonically increasing with  $J_p$  is thus found in all  
58 materials. This can equivalently be expressed in terms of an effective path length similarly increasing with  $J_p$ .

## 59 2. Experimental method

61 The magnetic measurements were performed at 50 Hz under sinusoidal induction waveform on the NO and GO  
62 alloys listed in Table 1. Both conventional (CGO) and high-permeability (HGO) grain-oriented sheets were  
63 investigated. A calibrated hysteresisgraph-wattmeter with digital control of the induction waveform was used,  
64 where signal acquisition and A/D conversion is made by means of a 12-bit 500 MHz HDO4054 LeCroy  
65 oscilloscope. The whole measuring process is performed within an Agilent VEE environment. The NO and GO  
66 alloys were tested in the polarization intervals 0.5 T – 1.5 T and 1.0 T – 1.8 T, respectively, with either eight or

67 twelve strips inserted in the Epstein frame, depending on the sheet thickness. For any given material, a standard  
 68 measurement was first made, followed by measurements with the centrally placed local windings. The  
 69 arrangement of the 17 mm wide  $H$ - and  $B$ -coils, which are stuck together and placed inside the Epstein windings,  
 70 is schematically shown in Fig. 1. The  $H$ -coil (turn-area  $N_{\text{H}}S_{\text{H}} = 2.11 \cdot 10^{-2} \text{ m}^2$ , thickness  $\sim 1.5 \text{ mm}$ ) is made of a few  
 71 hundred turns (wire diameter 0.05 mm) wound on a rigid fibreglass plate and calibrated inside a field reference  
 72 setup [10]. The 50-turn  $B$ -coil enwraps the  $H$ -coil and the strips under test. The air-flux contribution is usually  
 73 negligible, but it is in any case compensated via software. Once the single standard Epstein measurement of the  
 74 power loss  $P_{\text{epst}}(J_{0\text{p}})$  at a given polarization  $J_{0\text{p}}$  is done, the local  $\text{d}B/\text{d}t$  and  $\text{d}H_{\text{eff}}/\text{d}t$  signals are simultaneously  
 75 detected, under the identical exciting conditions, at a significant number of points, from corner to corner, along  
 76 the length of the Epstein leg, amplified by calibrated low-noise amplifiers SR560, and integrated. These local  
 77 measurements are then identically repeated on the other legs and the results are averaged. They provide the  
 78 behaviours of  $J(x)$  and  $H_{\text{eff}}(x)$  as a function of the distance  $x$  from the centre of the leg for the Epstein measured  
 79 polarization  $J_{0\text{p}}$ . The distance  $x$  ranges between -110 mm and +110 mm. Finally, the  $H$ - and  $B$ -coils are moved to  
 80 the centre of the leg ( $x = 0$ ) and the measurement of  $P_{\text{eff}}(J_{0\text{p}})$  is performed by imposing the local  $\text{d}J/\text{d}t$  sinusoidal  
 81 with peak polarization value  $J_{\text{p}}(0) = J_{0\text{p}}$ . It is remarked that across the 17 mm wide region occupied by the coils  
 82 centred at  $x = 0$  the polarization is highly uniform. Given the low field levels involved, a certain background noise  
 83 in the  $\text{d}H_{\text{eff}}/\text{d}t$  signal is inevitable. This is dealt with by repeating the very same measurement a number of times,  
 84 to make the random uncertainty contribution negligible. The process is further repeated on the other legs and the  
 85 results are averaged.

86

87

### 88 3. Experimental results and discussion

89 The general outcome of the measurements performed on the six different types of soft magnetic steels  
 90 described in Table 1, two NO sheets of thickness 0.194 mm and 0.343 mm, two conventional and two high-  
 91 permeability GO sheets, of thickness ranging between 0.255 and 0.295 mm, is that the standard Epstein loss figure  
 92  $P_{\text{epst}}$  can either overestimate or underestimate the effective power loss  $P_{\text{eff}}$ , but the ratio  $P_{\text{epst}} / P_{\text{eff}}$  is always a  
 93 monotonically increasing function of  $J_{\text{p}}$ . **The local  $J_{\text{p}} = J_{\text{p}}(0)$  value involved in the measurement of  $P_{\text{eff}}$  is obviously**  
 94 **made to coincide with the polarization value  $J_{0\text{p}}$  previously determined through the whole Epstein secondary**  
 95 **winding.** While this result may appear partly ad odd with previous literature outcomes [5][8], we shall observe in  
 96 the following how the behavior of  $P_{\text{epst}} / P_{\text{eff}}$  can be justified in terms of inhomogeneity of the induction along the  
 97 Epstein legs **and the power law dependence** of  $P_{\text{eff}}$  on  $J_{\text{p}}$ . Let us therefore observe in Fig. 2 the overall experimental  
 98 behaviors of  $(P_{\text{epst}} - P_{\text{eff}}) / P_{\text{eff}}$  versus  $J_{\text{p}}$  and of the related effective magnetic path length  $l_{\text{eff}} = l_{\text{m}} \cdot (P_{\text{epst}} / P_{\text{eff}})$ . **Similar**  
 99 **trends versus  $J_{\text{p}}$  are followed by the NO and GO materials, but the standard power loss  $P_{\text{epst}}$  becomes significantly**  
 100 **higher, around 4 % – 5 %, than the true loss  $P_{\text{eff}}$  at the highest  $J_{\text{p}}$  values in the GO sheets.** Table 2 provides a  
 101 comparison of the measured power losses  $P_{\text{epst}}$  and  $P_{\text{eff}}$ .

102 In order to find a rationale for the  $J_{\text{p}}$  dependent relationship between  $P_{\text{epst}}$  and  $P_{\text{eff}}$ , it is useful to analyze the

103 distribution of field and polarization along the magnetic circuit, as retrieved by the previously described local  
 104 measurements. To start with, we provide an example in Fig. 3, concerning the NO-2 sheet, of field decomposition  
 105 along a leg of the frame for a standard Epstein measurement at a given polarization value  $J_p$ . The solenoid  
 106 surrounding each leg has length  $2L = 195$  mm. By subtracting the effective field  $H_{\text{eff}}(x)$ , measured by sliding the  
 107  $H$ -coil along the leg, from the field  $H_{\text{sol}}(x)$  applied by the primary solenoid, we obtain the behavior of the  
 108 magnetostatic field  $H_d(x)$ . This exerts a demagnetizing action towards the strip portion of length  $2L$  underlying the  
 109 Epstein winding, adding instead to  $H_{\text{sol}}$  towards the corners, to eventually impose a magnetic path length  $l_{\text{eff}}$  longer  
 110 than the solenoid length. The effect of  $H_d$  is less important at high inductions, where the permeability is lower and  
 111 the free poles are more localized around the solenoid edges. The distribution of the polarization  $J_p(x)$  along  $2L$  is  
 112 however moderately affected, as shown by the examples regarding the samples NO-2 and HGO-1 shown in Fig.  
 113 4. These curves are representative of the flux distribution found in all materials and bring to light the fact that,  
 114 because of the strong non-linear dependence of the power loss on  $J_p$ , the true loss value cannot be recovered by a  
 115 standard Epstein measurement, adjusted through a simple constant (in this case the conventional magnetic path  
 116 length  $l_m$ ). By denoting the polarization measured through the secondary Epstein winding  $J_0(t) = J_{0p} \sin(\omega t)$ ,

117 where  $J_{0p} = \frac{1}{2L} \int_{-L}^L J_p(x) dx$ , we can write the power loss per unit volume measured with the standard method

$$118 \quad P_{\text{epst}}(J_{0p}) = \frac{1}{T} \int_0^T H_{\text{epst}}(t) \cdot J_{0p} \omega \cos(\omega t) dt, \quad (2)$$

119 where  $H_{\text{epst}}(t) = N_H i_H(t) / l_m$ ,  $N_H$  is the number of turns of the primary winding and  $i_H(t)$  is the magnetizing current.  
 120 The true power loss corresponding to the condition met with the standard Epstein measurement is therefore given  
 121 by the average of the local  $P_{\text{eff}}(x)$  across the length  $2L$

$$122 \quad P_{\text{eff}}(J_{0p}) = \frac{1}{2L} \int_{-L}^L dx \frac{1}{T} \int_0^T H_{\text{eff}}(t, x) \cdot J_p(x) \cdot \omega \cos(\omega t) dt = \frac{1}{2L} \int_{-L}^L P_{\text{eff}}(J_p(x)) dx. \quad (3)$$

123 We thus obtain the effective magnetic path length corresponding to such condition

$$124 \quad l_{\text{eff}}(J_{0p}) = l_m \cdot \frac{P_{\text{epst}}(J_{0p})}{P_{\text{eff}}(J_{0p})}. \quad (4)$$

125 The quantity  $P_{\text{eff}}(J_{0p})$  can be measured, according to Eq. (3), by integrating the previously discussed local  
 126 measurements, which are represented as a function of  $J_p$  in Fig. 5, over the  $J_p(x)$  distribution shown in Fig. 4. This  
 127 is easily done through knowledge of the measured dependence of  $P_{\text{eff}}(J_p)$  on  $J_p$ , which, as shown in Fig. 5, follows  
 128 a power law  $P_{\text{eff}}(J_p) \propto J_p^n$ , with  $n$  an increasing function of  $J_p$ . By introducing the  $P_{\text{eff}}(J_{0p})$  calculated by Eq. (3), we  
 129 obtain the behavior of  $l_{\text{eff}}(J_{0p})$  in the different materials shown in Fig. 6. On the other hand, the previously defined  
 130  $P_{\text{eff}}(J_p)$  (Fig. 2) is the true loss measured at  $x = 0$  when  $J_p(0) = J_p$ , which is compared with the Epstein power loss  
 131 when the secondary winding provides the same polarization value  $J_p$ .  $l_{\text{eff}}(J_p)$  is correspondingly defined through  
 132 Eq. (1). Consequently,  $l_{\text{eff}}(J_{0p})$  and  $l_{\text{eff}}(J_p)$  do not usually coincide.  $l_{\text{eff}}(J_{0p})$  is, in any case, the magnetic path length  
 133 to be applied in substitution of  $l_m$  when making the standard Epstein testing at 50 Hz at the specific measured

134 polarization level  $J_{0p}$ . It takes into account the fact that the peak polarization  $J_{0p}$  measured by the secondary Epstein  
135 winding is the average of  $J_p(x)$  between  $\pm L$ , according to the behaviors of  $J_p(x)$  shown in Fig. 4. It will coincide  
136 with  $l_{\text{eff}}(J_p)$  for homogeneous  $J_p(x)$  across the solenoid length  $2L$ , a limiting unattainable condition. The calculated  
137  $l_{\text{eff}}(J_{0p})$  and the measured  $l_{\text{eff}}(J_p)$  nevertheless display quite similar increasing trends vs.  $J_p$ , both in NO and GO  
138 alloys, as illustrated by their behaviors shown in Fig. 6. **It is appreciated the fact that, as shown in Figs. 2 and 6,**  
139 **the effective magnetic path length in the GO alloys tends to be higher than in the NO sheets, besides being larger**  
140 **than the conventional Epstein value  $l_m = 0.94$  m. This implies that  $P_{\text{epst}} / P_{\text{eff}}$  is similarly higher. The present results**  
141 **actually show that  $J_p(x)$  is more homogeneous in the GO strips (see the example shown in Fig. 4), thereby better**  
142 **approaching the ideal condition of perfectly homogeneous magnetization over the whole 1m long Epstein circuit.**  
143

#### 144 4. Conclusions

145 Measurements of the true power losses in different types of non-oriented and grain-oriented materials  
146 using localized  $H$ - and  $B$ -coils placed inside the legs of a standard 25 cm Epstein frame have been compared,  
147 upon a range of peak polarization values, with the loss figures obtained according to the usual procedure  
148 prescribed by the measuring standards. It is found that true  $P_{\text{eff}}$  and standard  $P_{\text{epst}}$  power loss figures are in a  
149 relationship dependent on the imposed peak polarization value  $J_p$ , with the ratio  $P_{\text{epst}} / P_{\text{eff}}$  exhibiting a  
150 monotonical increase with  $J_p$  in all materials in the investigated polarization range  $0.5 \text{ T} \leq J_p \leq 1.8 \text{ T}$ . This  
151 behavior, which can be interpreted in terms of an effective magnetic path length  $l_{\text{eff}}$ , to be used as a substitute for  
152 the conventional fixed length  $l_m = 0.94$  m in the expression for the applied field, is justified in terms of non-  
153 uniform profile of the polarization  $J_p(x)$  along the strip portion underlying the Epstein secondary winding and  
154 non-linear increase of  $P_{\text{eff}}$  with  $J_p$ . The effective path length  $l_{\text{eff}}(J_p)$  can then be calculated, by which true and  
155 Epstein power losses are reconciled.

156

157

158

159

160

161

162

163

164

165

166

167

168

169

170  
171  
172  
173  
174  
175  
176  
177  
178  
179  
180  
181  
182  
183  
184  
185  
186  
187  
188  
189  
190  
191  
192  
193  
194  
195  
196  
197  
198  
199  
200  
201  
202  
203  
204  
205  
206  
207  
208  
209  
210  
211

## References

- [1] J. Sievert, H. Ahlers, F. Fiorillo, L. Rocchino, M. Hall and L. Henderson, Magnetic measurements on electrical steels using Epstein and SST method, *PTB-Bericht E-74*(2001), 1–28.
- [2] C. Appino, E. Ferrara, F. Fiorillo, L. Rocchino, C. Ragusa, J. Sievert, T. Belgrand, C. Wang, P. Denke, S. Siebert, Y. Norgren, K. Gramm, S. Norman, R. Lyke, M. Albrecht, X. Zhou, W. Fan, X. Guo, M. Hall, “International comparison on SST and Epstein measurements in grain-oriented Fe-Si sheet steel”, *Int. J. Appl. Electromagnetics Mech.* **48** (2015), 123-133, doi: 10.3233/JAE-151978.
- [3] IEC Standard Publication 60404-2, Methods of measurement of the magnetic properties of electrical steel sheet and strip by means of the Epstein frame, (Geneva: IEC Central Office, 1996).
- [4] ASTM Publication A343.97, Standard test method for alternating-current magnetic properties of amorphous materials at power frequencies using wattmeter-ammeter-voltmeter method using wattmeter-ammeter-voltmeter method and 25-cm Epstein test frame” (West Conshohocken, PA: ASTM International, 1993).
- [5] J.D. Sievert, Determination of the AC magnetic power loss of electrical steel sheet: present status and trends, *IEEE Trans. Magn.* **20** (1984), 1702-1706, doi: [10.1109/TMAG.1984.1063278](https://doi.org/10.1109/TMAG.1984.1063278).
- [6] E. Antonelli, E. Cardelli, A. Faba, Epstein frame: how and when it can be really representative about the magnetic behavior of laminated magnetic steels, *IEEE Trans. Magn.* **41** (2005), 1516-1519, doi: [10.1109/TMAG.2005.845072](https://doi.org/10.1109/TMAG.2005.845072).
- [7] P. Marketos, S. Zurek, and A.J. Moses, A method for defining the mean path length of the Epstein frame, *IEEE Trans. Magn.* **43** (2007), 2755-2757, doi: [10.1109/TMAG.2007.894124](https://doi.org/10.1109/TMAG.2007.894124).
- [8] H. Ahlers, J.D. Sievert, and Qu.-ch. Qu, Comparison of a single strip tester and Epstein frame measurements, *J. Magn. Magn. Mater.* **26** (1982), 176-178, doi:10.1016/0304-8853(82)90145-7.
- [9] P. Marketos, S. Zurek, and A.J. Moses, Calculation of the mean path length of the Epstein frame under non-sinusoidal excitations using the double Epstein method, *J. Magn. Magn. Mater.*, **320** (2008), 2542-2545, doi: [10.1016/j.jmmm.2008.04.085](https://doi.org/10.1016/j.jmmm.2008.04.085).
- [10] F. Fiorillo, G.F. Durin, and L. Rocchino: “A reference system for the measurement of low-strength magnetic flux density”, *J. Magn. Magn. Mater.*, **304** (2006), e540-e542.



212  
213  
214  
215  
216  
217  
218  
219  
220  
221  
222  
223  
224  
225  
226  
227  
228  
229  
230  
231  
232  
233  
234  
235  
236  
237  
238  
239  
240  
241  
242  
243  
244  
245  
246  
247  
248  
249  
250  
251  
252  
253  
254  
255  
256  
257  
258  
259  
260  
261  
262  
263  
264

Table 1  
Physical parameters of the investigated non-oriented (NO), conventional (CGO) and high-permeability (HGO) grain-oriented steel sheets.

Fe-Si alloy	Composition	Thickness (mm)	Density (kg/m <sup>3</sup> )	Resistivity (mΩm)
NO-1	Fe-(3.2 wt%)Si	0.194	7650	52·10 <sup>-8</sup>
NO-2	Fe-(3.5 wt%)Si	0.343	7600	56.4·10 <sup>-8</sup>
CGO-1	Fe-(3 wt%)Si	0.255	7650	48·10 <sup>-8</sup>
CGO-2		0.261		
HGO-1		0.257		
HGO-2		0.295		

265  
 266  
 267  
 268  
 269  
 270  
 271  
 272  
 273  
 274  
 275  
 276  
 277  
 278  
 279  
 280  
 281  
 282  
 283  
 284  
 285  
 286  
 287

Table 2  
 Power loss at 50 Hz obtained by the standard Epstein measurement ( $P_{epst}$ ) and the localized measurement ( $P_{eff}$ ) as a function of peak polarization on three different Fe-Si sheets.

$f = 50 \text{ Hz}$	NO-1		CGO-2		HGO-1	
$J_p \text{ (T)}$	$P_{epst} \text{ (W/kg)}$	$P_{eff} \text{ (W/kg)}$	$P_{epst} \text{ (W/kg)}$	$P_{eff} \text{ (W/kg)}$	$P_{epst} \text{ (W/kg)}$	$P_{eff} \text{ (W/kg)}$
0.50	0.241	0.248	--	--	--	--
0.75	0.480	0.489	--	--	--	--
1.0	0.784	0.755	0.345	0.343	0.303	0.299
1.2	1.125	1.135	0.499	0.498	0.431	0.426
1.4	1.656	1.665	--	--	--	--
1.5	2.07	2.050	0.811	0.787	0.681	0.664
1.7	--	--	1.198	1.154	0.914	0.874
1.8	--	--	1.587	1.514	1.123	1.063

288  
 289  
 290  
 291  
 292  
 293  
 294  
 295  
 296  
 297  
 298  
 299  
 300  
 301  
 302  
 303  
 304  
 305  
 306

Figure captions

307  
308  
309  
310  
311  
312  
313  
314  
315  
316  
317  
318  
319  
320  
321  
322  
323  
324  
325  
326  
327  
328  
329  
330  
331  
332  
333  
334  
335  
336  
337  
338  
339  
340  
341  
342  
343  
344  
345  
346  
347  
348  
349  
350  
351  
352  
353  
354  
355  
356  
357

Fig. 1 – Arrangement of the local sensing coils inside a leg of the Epstein frame. The flat multiturn  $H$ -coil (thickness  $\sim 1.5$  mm) is placed in contact with the Epstein strip surface and the  $B$ -coil is wound around it and the steel strips. The coils are about 17 mm wide and can slide along the whole length of the Epstein leg.

Fig. 2 – The experimental dependence on  $J_p$  of the ratio of standard to true power losses  $P_{\text{epst}}/P_{\text{eff}}$  in NO and in conventional (CGO) and high-permeability (HGO) Fe-Si alloys (a) is paralleled by the behavior of the effective magnetic path length  $l_{\text{eff}}$  (b).

Fig. 3 – Effective field  $H_{\text{eff}}$  measured versus the distance  $x$  from the Epstein leg centre in the NO-2 sheet. It is  $H_{\text{eff}} = H_{\text{sol}} - H_d$ , the difference between the field  $H_{\text{sol}}$  generated by the primary winding and the field  $H_d$  originating from the free poles distributed along the strip length. To note the demagnetizing and magnetizing effect of  $H_d$  beneath and outside the solenoid length. The horizontal dotted line shows the conventional field  $H_{\text{epst}}$ , calculated assuming the magnetic path length  $l_m = 0.94$  m.

Fig. 4 – Examples of measured distribution of the reduced polarization  $J(x) / J(0)$  upon the portion of strip length underlying the Epstein secondary winding in the NO-2 and HGO-1 sheets.

Fig. 5 – The measured effective power loss  $P_{\text{eff}}(J_p)$  increases with the peak polarization  $J_p$  according to a power law  $P_{\text{eff}} \propto J_p^n$ , with  $n$  an increasing function of  $J_p$ .

Fig. 6 – Effective magnetic path lengths  $l_{\text{eff}}(J_{0p})$  and  $l_{\text{eff}}(J_p)$  versus peak polarization in the investigated NO and GO steel sheets.  $l_{\text{eff}}(J_{0p})$  is calculated through Eqs. (2)–(4). It permits one to retrieve the true power loss value from the standard loss figure for peak polarization  $J_{0p}$  measured with the secondary Epstein winding.  $l_{\text{eff}}(J_p)$  is the same quantity obtained for  $J_p = J_p(0)$ , where  $J_p(0)$  is the polarization measured at the centre of the Epstein leg.

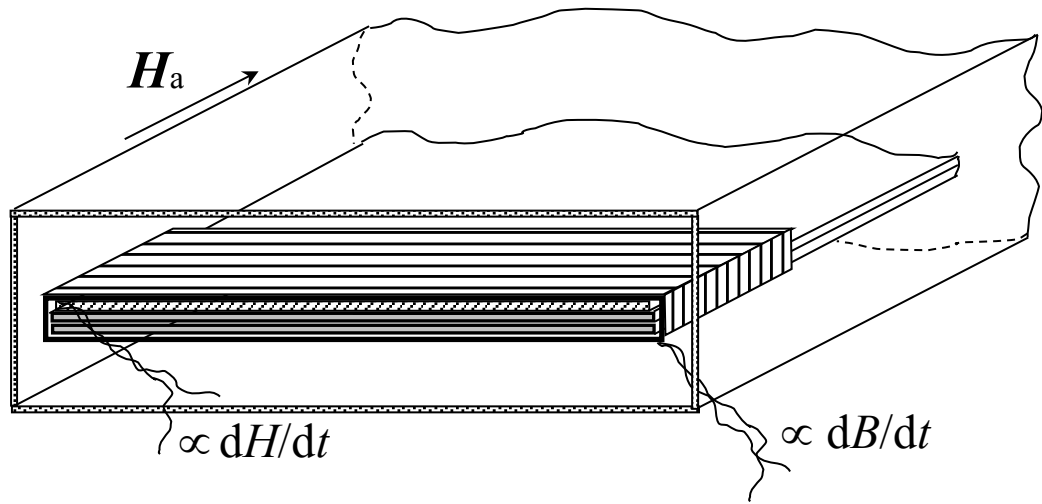
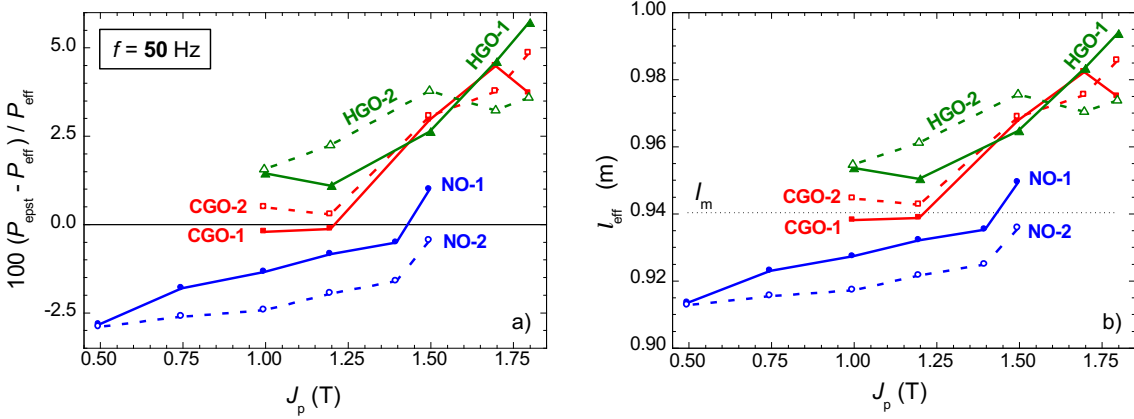


Fig. 1 – Arrangement of the local sensing coils inside a leg of the Epstein frame. The flat multiturn  $H$ -coil (thickness  $\sim 1.5$  mm) is placed in contact with the Epstein strip surface and the  $B$ -coil is wound around it and the steel strips. The coils are about 17 mm wide and can slide along the whole length of the Epstein leg.

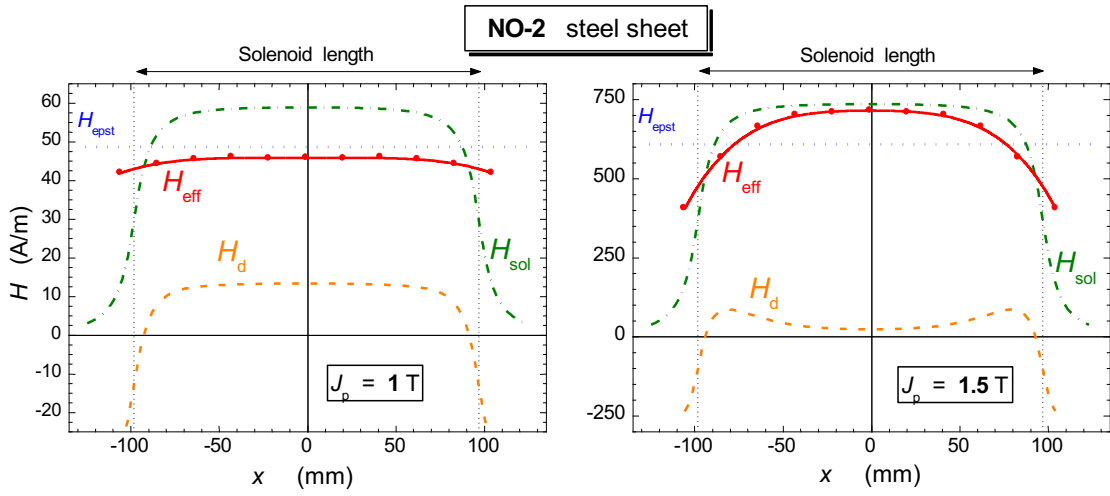
408  
 409  
 410  
 411  
 412  
 413  
 414  
 415  
 416



417  
 418  
 419  
 420  
 421  
 422  
 423  
 424  
 425  
 426  
 427  
 428  
 429  
 430  
 431  
 432  
 433  
 434  
 435  
 436  
 437  
 438  
 439

Fig. 2 – The experimental dependence on  $J_p$  of the ratio of standard to true power losses  $P_{epst}/P_{eff}$  in NO and in conventional (CGO) and high-permeability (HGO) Fe-Si alloys (a) is paralleled by the behavior of the effective magnetic path length  $l_{eff}$  (b).

440  
441  
442  
443  
444  
445  
446



447  
448  
449  
450  
451  
452  
453  
454  
455  
456  
457  
458  
459  
460  
461  
462  
463  
464  
465

leg 466  
 $H_{\text{sol}}$  467  
les 468  
ing 469  
ine 470  
gth 471  
472  
473  
474  
475  
476  
477  
478  
479  
480  
481  
482  
483  
484  
485  
486  
487  
488

489  
490  
491  
492  
493  
494  
495  
496  
497  
498  
499  
500  
501  
502  
503  
504  
505  
506  
507  
508  
509  
510  
511  
512  
513  
514  
515  
516  
517  
518  
519  
520  
521  
522  
523  
524  
525  
526  
527  
528  
529  
530  
531  
532  
533  
534  
535  
536  
537

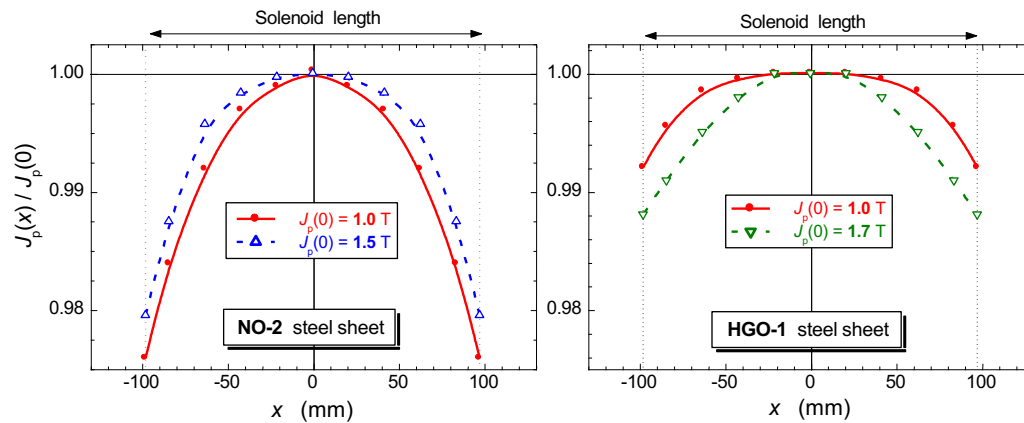


Fig. 4 – Examples of measured distribution of the reduced polarization  $J(x) / J(0)$  upon the portion of strip length underlying the Epstein secondary winding in the NO-2 and HGO-1 sheets.

538  
 539  
 540  
 541  
 542  
 543  
 544  
 545  
 546  
 547  
 548  
 549  
 550  
 551  
 552  
 553  
 554  
 555  
 556  
 557  
 558  
 559  
 560  
 561  
 562  
 563  
 564  
 565  
 566  
 567  
 568  
 569  
 570  
 571  
 572  
 573  
 574  
 575  
 576  
 577  
 578  
 579  
 580  
 581  
 582  
 583  
 584  
 585  
 586

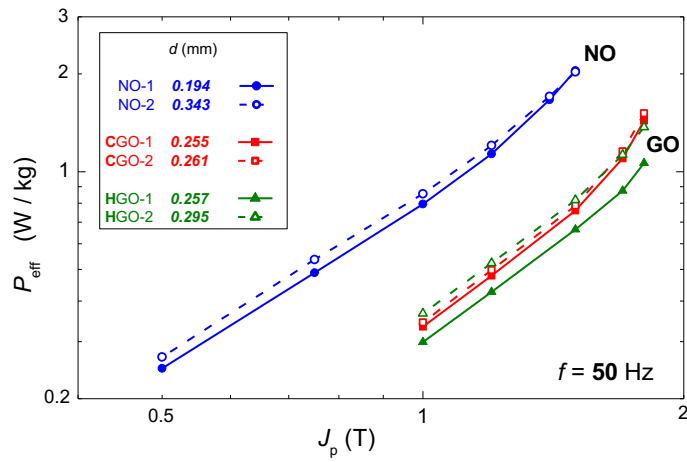
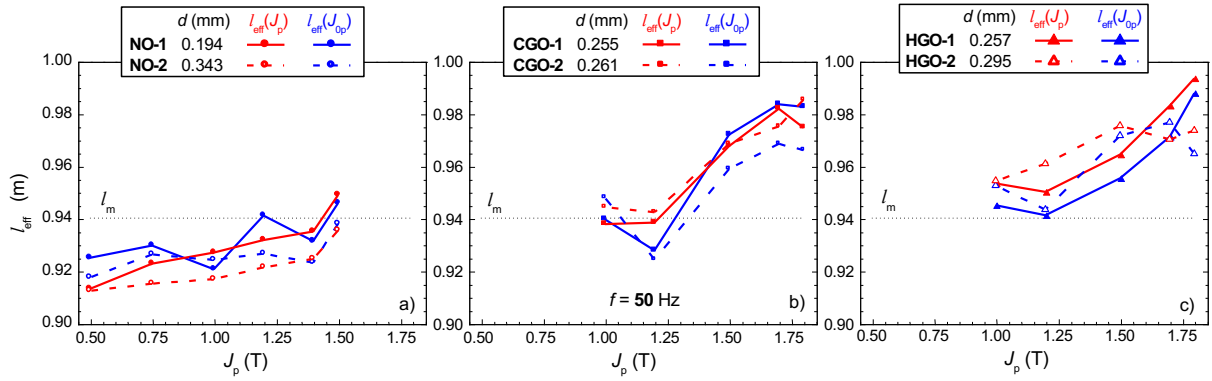


Fig. 5 – The measured effective power loss  $P_{\text{eff}}(J_p)$  increases with the peak polarization  $J_p$  according to a power law  $P_{\text{eff}} \propto J_p^n$ , with  $n$  an increasing function of  $J_p$ .



587  
 588  
 589  
 590  
 591  
 592  
 593  
 594  
 595  
 596



597  
 598  
 599  
 600  
 601  
 602  
 603  
 604  
 605

Fig. 6 – Effective magnetic path lengths  $l_{\text{eff}}(J_{0p})$  and  $l_{\text{eff}}(J_p)$  versus peak polarization in the investigated NO and GO steel sheets.  $l_{\text{eff}}(J_{0p})$  is calculated through Eqs. (2)–(4). It permits one to retrieve the true power loss value from the standard loss figure for peak polarization  $J_{0p}$  measured with the secondary Epstein winding.  $l_{\text{eff}}(J_p)$  is the same quantity obtained for  $J_p = J_p(0)$ , where  $J_p(0)$  is the polarization measured at the centre of the Epstein leg.